JOURNAL OF MAGNETIC RESONANCE **131,** 118–125 (1998)
ARTICLE NO. MN971333

Flip Angle Effects in STEAM and PRESS—Optimized versus Sinc RF Pulses

Lawrence N. Ryner,* Yong Ke,† and M. Albert Thomas†

**Institute for Biodiagnostics, National Research Council, Winnipeg, Manitoba, Canada; and †Department of Radiological Sciences, University of California, Los Angeles, California 90095*

Received June 5, 1997; November 20, 1997

Flip angle dependence of the localized single-voxel ^{1}H NMR spectroscopic sequences STEAM and PRESS using numerically optimized Shinnar–Le Roux (SLR) and conventional sinc RF pulses has been evaluated. Phantom experiments were used to evaluate voxel profiles from MR images of the selected voxels. Information on the total excited volume was recorded from the integrated area under the water peak in the localized spectrum at different flip angles ($\theta = 0°–180°$). The voxel profiles for both the STEAM and PRESS sequences using the SLR RF pulses were found to be identical, unlike the case for the sinc RF pulses. The SLR RF pulses in the PRESS sequence were found to be more sensitive to flip angle variations. Localized, water-suppressed ^{1}H NMR spectra recorded from the frontal gray matter in healthy volunteers ($n = 3$) showed less lipid contamination using the SLR RF pulses compared with the sinc RF pulses. © 1998 Academic Press

Key Words: **flip angle localized NMR spectroscopy.**

INTRODUCTION

Slice-selective excitation using a variety of shaped radio-frequency (RF) waveforms in combination with magnetic field gradients is an important area of research in both magnetic resonance imaging (MRI) and spectroscopy (MRS). In many spin-echo-based MRI and MRS pulse sequences, both the 90° excitation and the 180° refocusing RF pulses are slice-selective (*1–10*). The difficulties associated with producing optimal slice profiles with 180° refocusing RF pulses have been well documented (*1–6, 10*).

The Shinnar–Le Roux (SLR) selective excitation pulse design algorithm was originally proposed by Shinnar and Le Roux, and put in usable form by Pauly and Le Roux. Macovski and co-workers have presented a mathematical basis for pulse design and an efficient algorithm for computing a variety of optimized RF pulses (*7, 8*). The performance of 90° and 180° RF pulses used in spin-echo-based sequences and chemical-shift-selective saturation pulses has been reported.

In localized ^{1}H magnetic resonance spectroscopy, the stimulated echo acquisition mode (STEAM) and point-resolved spectroscopy (PRESS) pulse sequences are the voxel localization methods of choice (*11, 12*). This arises from an ability to acquire single-excitation localized spectra with easy implementation of water and fat suppression pulses (*13–16*). Moonen *et al.* used several criteria in comparing the two sequences, including the actual size of the selected volume, sensitivity to spin displacement, and other related issues. They found, using the conventional sinc RF pulses, that the actual volume selected by STEAM was 67% higher than that selected by PRESS (*14*).

With the implementation of new RF pulses numerically optimized using the Shinnar–Le Roux algorithm on a conventional whole-body NMR scanner (*17*), the differences in excited volumes and slice profiles between the STEAM and PRESS techniques at flip angles $\theta_{1,2,3} = 90°$ and $\theta_{1,2,3} \neq 90°$ for STEAM and [$\theta_1 = 90°$ $\theta_{2,3} = 180°$ and $\theta_1 \neq 90°$ $\theta_{2,3} \neq 180°$] for PRESS have not yet been reported. The goals of this work were (a) to record the voxel profiles localized by STEAM and PRESS using the SLR and sinc RF pulses, (b) to compare the sensitivity to flip angle variation of the numerically optimized SLR RF pulses with the conventional sinc RF pulses, and (c) to compare the contamination of intracranial lipids in healthy volunteers using the STEAM/PRESS sequences with the SLR and sinc RF pulses.

MATERIALS AND METHODS

All experiments were performed on a 1.5-T whole-body MR scanner (Signa, General Electric, Milwaukee, WI) equipped with self-shielded gradient coils. The two pulse sequences studied were the standard product STEAM and PRESS sequences. The SLR versions of the two sequences were originally developed by GE Medical Systems while the sinc versions were locally implemented. Phantom and *in vivo* studies were carried out at the University of Wisconsin Clinical Science MR Center and the University of California, Los Angeles (UCLA), Medical Center MR facility, respectively (both sites had exactly the same make and model of

1090-7807/98 $25.00

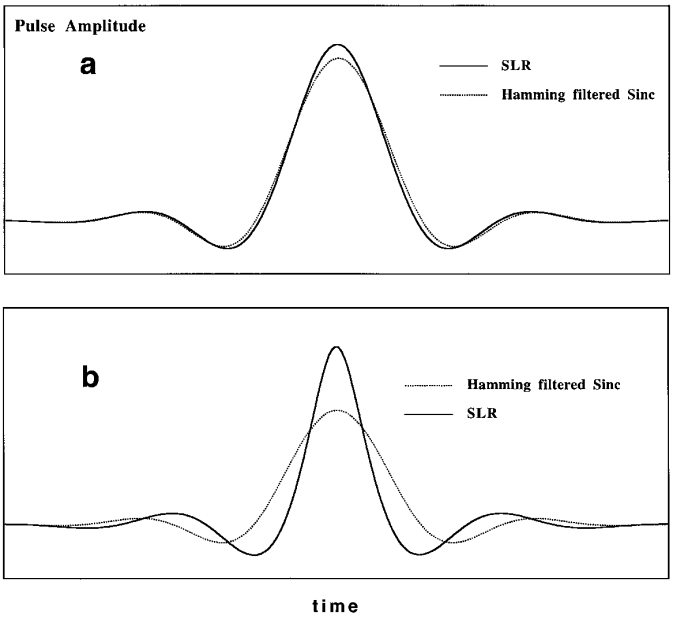

FIG. 1. (a) SLR/sinc 90° and (b) SLR/sinc 180° RF waveforms used in STEAM and PRESS. Three four-zero truncated sinc RF pulses, 1.6 ms each, were used for the 90° excitation pulses in STEAM-sinc version, and 3.2-ms RF pulses were used for both the 90° and 180° RF pulses in the PRESS-sinc version. In the STEAM-SLR version, the 90° RF pulses were 1.8 ms in length. In the PRESS-SLR version, the durations of the 90° and 180° RF pulses were 3.6 and 7.8 ms, respectively.

MR scanner). The *in vitro* results were reproduced in both facilities (*18*).

The RF pulses studied are shown in Fig. 1: (a) the SLR-optimized 90° RF pulse and the conventional Hamming-windowed sinc RF pulse; (b) the SLR-optimized 180° RF pulse and the conventional Hamming-windowed sinc RF pulse. The durations of the four-zero truncated sinc 90° RF pulses in the STEAM and PRESS sequences were 1.6 and 3.2 ms, respectively. The sinc 180° RF pulse was also 3.2 ms long in the PRESS sequence. The SLR 90° RF pulse was 1.8 ms long in the STEAM sequence. The durations of the SLR 90°/180° RF pulses were 3.6 and 7.8 ms, respectively, in the PRESS sequence. The minimum echo time (TE) for the PRESS-sinc RF pulse sequence was 35 ms versus 65 ms with the PRESS-SLR version due to the longer duration of the SLR RF pulses and crusher gradient pulses. This could be reduced by decreasing the duration of the crusher gradients through the use of a higher gradient strength of 23 mT/M (*19*).

A 1-liter spherical phantom containing water doped with $CuSO_4$ (Fisher Scientific Co., New Jersey) at a concentration of 1.4 mM was positioned in a quadrature transmit/receive head coil. A standard spin-echo localizer MR image was acquired. Using the imaging capabilities of the STEAM pulse sequence, an image of an 8-ml cubic volume localized in the center of the phantom was obtained. The RF amplifier gain setting was determined for a 90° pulse by maximizing the signal while attempting to maintain an ideal voxel profile (flat top, sharp transition regions on each side). A water spectrum from the selected volume was subsequently acquired using the spectroscopy mode of the STEAM pulse sequence (without read or phase-encoding gradients). The flip angle was varied by altering the gain setting on the RF amplifier. A spectrum and an MR image were acquired for each flip angle setting. The spectra provided information as to the variation of the total signal from the voxel as a function of flip angle. The MR images displayed the spatial variation of the voxel profile as a function of flip angle. This entire sequence was then repeated using the PRESS pulse sequence.

Details of the acquisition parameters for both STEAM and PRESS include TE = 65 ms and TR = 2000 ms. It is evident that an insufficient repetition time could lead to partial saturation of magnetization (*20*). We measured T_1 of (a) pure water and (b) water doped with $CuSO_4$ at a concentration of 1.4 mM, and they were 2.8 and 1.2 s, respectively. A 256 × 256 image matrix was acquired in approximately 9 min. Spectroscopy acquisition parameters included a spectral width of 2500 Hz and 2048 points per acquisition. The full width at half-maximum of the water resonance for all spectra was approximately 2 Hz. An apodization filter of 2 Hz exponential line broadening was applied to each free-induction decay after zero-filling to 4096 points. The area under the water resonance was calculated by integration.

The expected sharper voxel profiles with the SLR RF pulses versus the sinc RF pulses should give rise to reduced spectral lipid contamination for a voxel positioned close to the skull marrow. In order to investigate this effect, an 18-ml voxel was localized in the frontal gray/white matter region of healthy volunteers (n = 3). The spectra from the STEAM sequence using the SLR and the sinc RF pulses were compared. The following parameters were used: TR/TE = 1500 ms/20 ms, total number of excitations (NEX) = 128, and CHESS water suppression (three consecutive frequency-selective RF pulses followed by dephasing B_0 gradient pulses). In the STEAM/SLR sequence, the RF pulses in the CHESS sequence were also SLR RF pulses.

A software package developed by GE Medical Systems (Milwaukee, WI) was used to process the cerebral ^{1}H MR spectra which were processed with the following parameters: (1) apodization with an exponential filter (2 Hz line broadening) and (2) zero-filling the raw data from 2048 to 4096 complex points and fast Fourier transformation to obtain the spectral frequencies. Water signal was used to correct the phase of the metabolite peaks in the time domain.

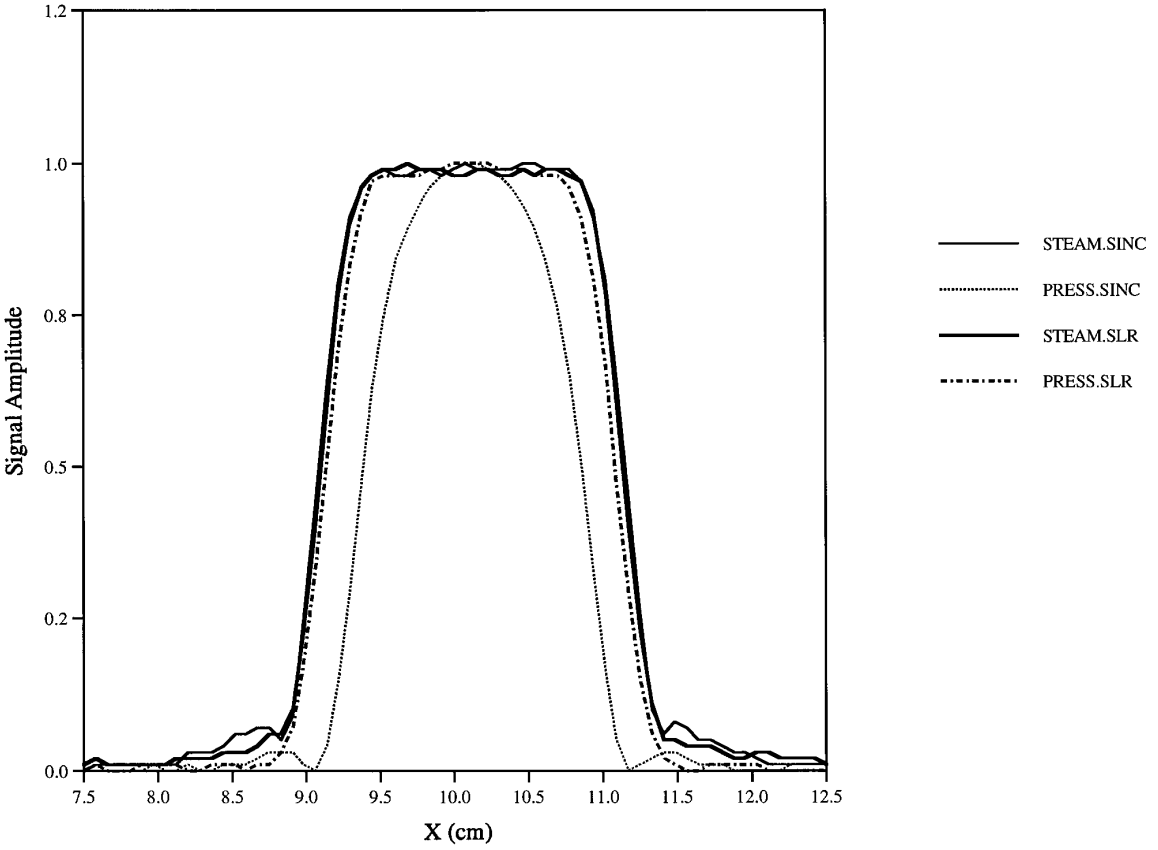

FIG. 2. Voxel spatial profiles, extracted from the central row of pixels in each of the voxel images, for STEAM-SLR, STEAM-SINC, PRESS-SLR, and PRESS-SINC pulse sequences at a flip angle of 90° for STEAM and 90°/180° for PRESS.

Informed consent was obtained from each volunteer prior to the examination in accordance with human ethics committee guidelines.

RESULTS AND DISCUSSION

90°/180° Flip Angle Voxel Profiles

Figure 2 shows the voxel profiles for the STEAM and PRESS pulse sequences using SLR and sinc RF pulses with the flip angle set at 90° (90° and 180° for PRESS). These profiles were obtained by extracting the central row passing through the middle of the voxel from each of the voxel images. Note the extremely flat top of the SLR voxel profile as compared with that of the sinc pulse. This is important to ensure that metabolites will be uniformly excited across the dimensions of the voxel. Also notice the sharp transition region at the edge of the voxel. This is important to ensure that all signal arises from the selected voxel and not a blurred region in the general area of the selected volume. Very little signal was observed outside the selected volume whereas with a standard truncated sinc RF pulse, even though the transition region at the edge of the voxel was reasonably sharp, a region immediately adjacent to the selected region is excited to approximately 5% of the signal observed at the center of the voxel. This results in appreciable signal originating from outside the selected volume. In contrast to the nonoptimized RF pulse responses, the profiles for the optimized RF pulses are essentially identical for STEAM and PRESS. Using the full width at half-maximum (FWHM) of the profiles extracted from the central pixels shown in Fig. 2, our calculations showed the following: (a) the volume excited by the STEAM-sinc sequence was 65% more than that using the PRESS-sinc sequence, in conformity with the previous report (*14*), and (b) the volume excited by the STEAM-SLR sequence was 10% more than that using the PRESS-SLR sequence.

Flip Angle Dependence

The STEAM and PRESS localization techniques exhibited very different responses to variation of flip angle with respect to voxel profile and total signal. A complex relationship between the integrated signal and flip angle was observed

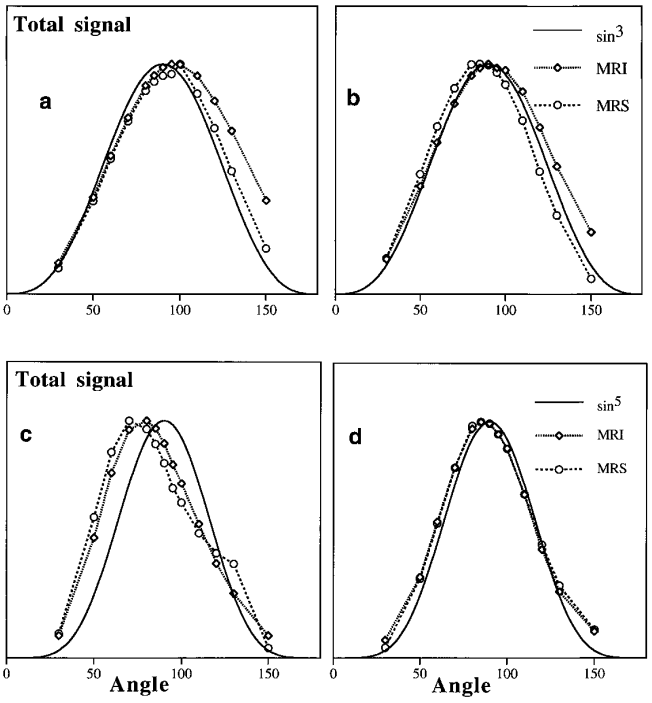

FIG. 3. Flip angle dependence of (a) STEAM-SLR, (b) STEAM-sinc, (c) PRESS-SLR, and (d) PRESS-sinc pulse sequences. The three curves plotted are the *total signal* as measured from the integrated area under the water peak in the MR spectra (MRS), the normalized gray scale value from the central pixel of the MR images (MRI), and the theoretical flip angle dependence ($\sin^3\theta$ for STEAM and $\sin^5\theta$ for PRESS, where θ is the flip angle of the three RF pulses in STEAM, and θ is the flip angle of the excitation pulse and 2θ is the flip angle of the refocusing pulse in PRESS).

with the SLR RF pulses compared to the simple $\sin^3(\theta)$ and $\sin^5(\theta)$ dependences with hard-pulse STEAM and PRESS sequences.

STEAM with SLR and sinc RF pulses. The experimental variation of *total signal*, as calculated from the area under the water resonance in the MR spectrum, as a function of flip angle (θ) showed close agreement to the theoretically expected $\sin^3\theta$ dependence of the STEAM signal (Fig. 3a using STEAM-SLR and Fig. 3b using STEAM-sinc sequences). It would appear that the flip angle setting with STEAM is not crucial since, aside from the desire to maximize signal at $\theta = 90°$, the total signal simply follows the $\sin^3\theta$ dependence as predicted theoretically. However, by observing the variation in voxel profile, where the central row of pixels from the voxel MR images has been extracted, as a function of flip angle (Fig. 4a using STEAM-SLR and Fig. 4b using STEAM-sinc sequences), it is clear that for $\theta > 90°$, significant degradation of the profile occurs, even though the total signal still follows a $\sin^3\theta$ dependence. The signal from the edges of the voxel does not decrease as fast as the signal from the middle of the voxel, with increasing flip angle, with the effect being most pronounced at the corners of the voxel. The slice profile degradation effect becomes significant for a flip angle error of approximately 7°–8°. For $\theta < 90°$, the voxel profile retains its flat top and sharp transition regions; however, the amplitude is decreased in agreement with the theoretical dependence. Increased signal from regions adjacent to the selected voxel is evident in the STEAM-sinc sequence as compared with the STEAM-SLR sequence. This effect is also appreciated in the three-dimensional (3D) surface plots derived from the voxel MR images for three different flip angle settings of 74° (A), 90° (B), and 110° (C) as shown in Fig. 5i for the STEAM-SLR (left) and STEAM-sinc (right) sequences.

PRESS with SLR and sinc RF pulses. A plot of *total signal*, as calculated from the area under the water resonance in the MR spectrum, versus flip angle for the PRESS-SLR sequence (Fig. 3c) exhibits very little agreement with the theoretical $\sin^5\theta$ dependence. Maximum signal occurs experimentally at a flip angle of 75° (corresponding to a 75°–150°–150° pulse sequence). A plot of the corresponding voxel profiles, taken from the central row of pixels in the voxel MR images, with varying flip angle is shown in Fig. 4c. At $\theta = 90°$, the voxel profile is ideal (flat top and sharp transition regions on the sides). For $\theta > 90°$, significant voxel profile degradation occurs with the signal from the edge of the voxel decreasing faster than the signal from the middle of the voxel and the addition of lobes outside the excited voxel. For $\theta < 90°$, again voxel profile degradation is observed with the signal from the edge of the voxel now decreasing slower than signal from the middle of the voxel. The 3D surface plots clearly demonstrate these effects as shown in Fig. 5ii. With PRESS-SLR, slice profile degradation becomes significant for a smaller flip angle error of approximately 2°–3°. The PRESS-SLR sequence is thus much more sensitive to flip angle variation as observed in the deterioration of voxel profile as compared with the STEAM sequence.

A plot of the signal at the exact center of the excited voxel versus flip angle shows a better correlation with the theoretical curve (central pixel curve in Fig. 3c). This suggests that the deviation from theoretical response of the total signal is due mainly to the increased volume localized by the SLR pulses. It should be noted that the RF pulses were optimized for a single flip angle setting of 90° (or 180° for two of the PRESS-SLR RF pulses) and were not optimized for other flip angles. The user must adjust the gain on the RF amplifier to match these optimum flip angles.

The fact that maximum total signal occurs for a flip angle of 75° has an important implication with regard to the setting of the flip angle with the PRESS-SLR sequence. In addition to the coarse method of setting the flip angle by calibration with respect to a rectangular RF pulse which excites the entire volume, two methods generally used for fine tuning

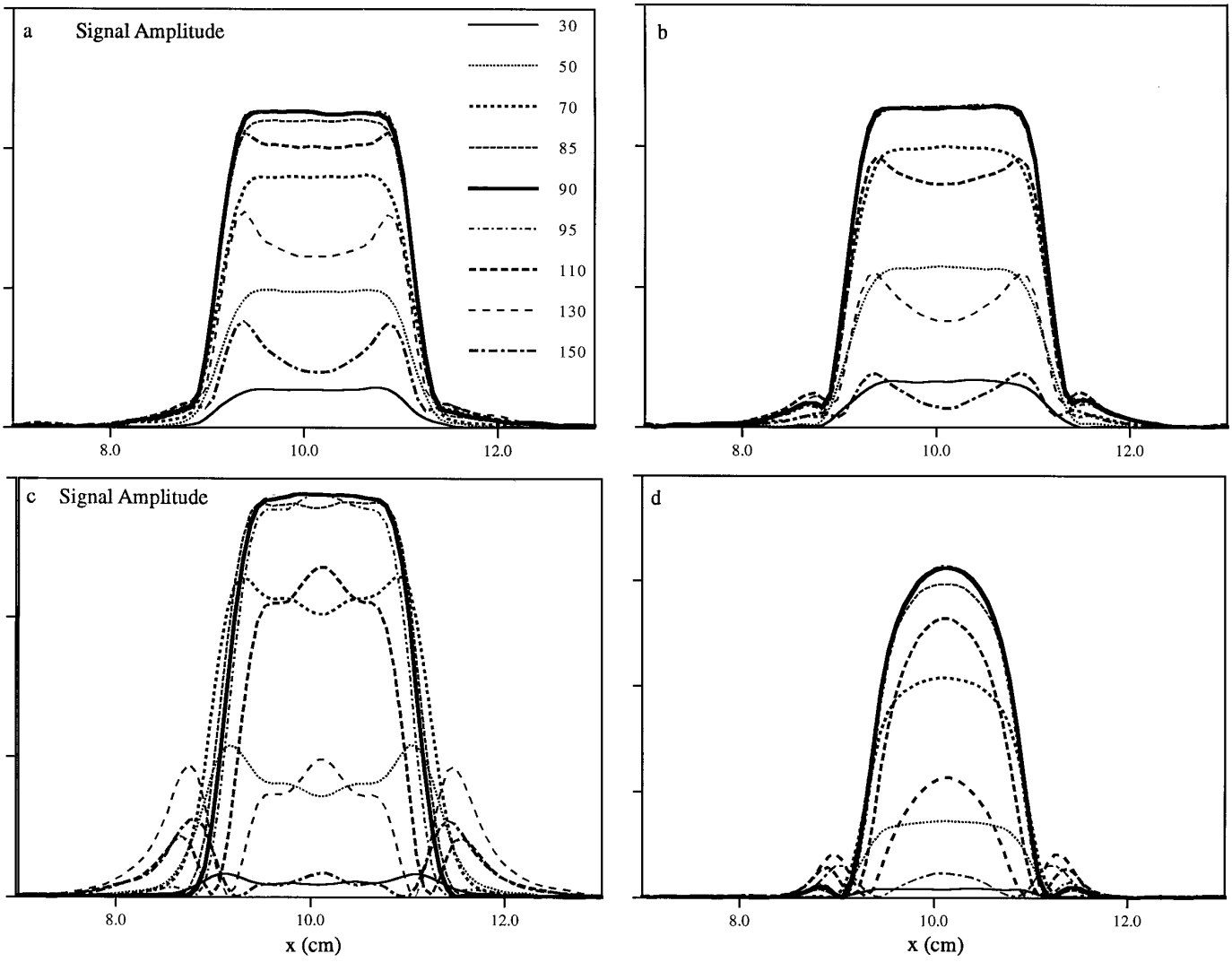

FIG. 4. Variation of voxel profile at different flip angles for (a) STEAM-SLR, (b) STEAM-sinc, (c) PRESS-SLR, and (d) PRESS-sinc pulse sequences. Plotted are the central row of pixels extracted from each of the MR voxel images recorded at θ = 30°, 50°, 70°, 85°, 90°, 95°, 110°, 130°, and 150°.

the 90° flip angle in spectroscopic pulse sequences are: (1) vary the RF amplifier gain setting while observing the MR spectrum until the maximum area under the water resonance is obtained and (2) vary the RF amplifier gain setting while observing the voxel profile until maximum signal consistent with a good voxel profile is obtained. Either method could be used with the STEAM sequence and the same gain setting would be achieved. However, if method 1 were used with the PRESS-SLR sequence it is clear that the severely degraded voxel profile corresponding to $\theta = 75°$ would result. It is imperative that the 90° flip angle be set according to method 2 with the PRESS-SLR sequence.

The experimental results of the *total signal*, as calculated from the area under the water resonance in the MR spectrum, versus flip angle for the PRESS-sinc sequence (Fig. 3d) show good correlation with the theoretical $\sin^5\theta$ dependence. A plot of the corresponding voxel profiles, taken from the central row of pixels in the voxel MR images, with varying flip angle is shown in Fig. 4d. Even at $\theta = 90°/180°$ the voxel profile is not flat-topped with sharp transition regions to zero signal outside the selected voxel. The contamination from the voxel boundaries is significant at $\theta > 90°$. This effect is again appreciated in the 3D surface plots derived from the voxel MR images for three different flip angle settings of 74°, 90°, and 110° (Fig. 5ii).

Flip angle sensitivity can be minimized using adiabatic RF pulses (*21–24*), which have been used extensively in surface coil transmission (*25, 26*). For slice selection in

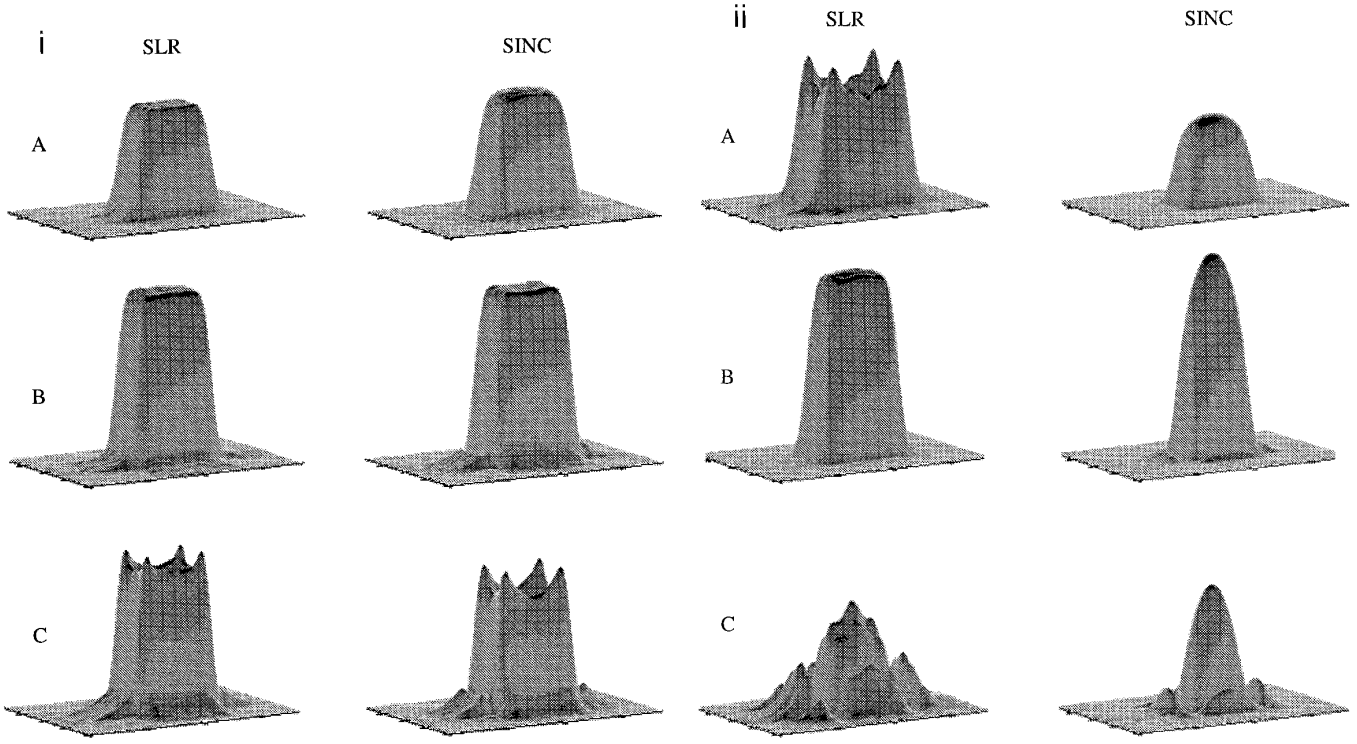

FIG. 5. 3D surface plots of voxel images for flip angles of 74° (A), 90° (B), and 110° (C) in (i) STEAM-SLR/STEAM-sinc and (ii) PRESS-SLR/PRESS-sinc pulse sequences.

PRESS and STEAM sequences, however, an adiabatic passage version of the numerically optimized SLR pulses has not yet been implemented and future work will address these problems.

MRS of Healthy Volunteers

The STEAM sequence with SLR and sinc RF pulses was investigated in three healthy volunteers. The axial MR image of a 25-year-old healthy volunteer is shown in Fig. 6c along with the location of the selected voxel (18-ml voxel in the frontal gray/white matter region). The spectrum shown in Fig. 6a was acquired with the STEAM-sinc RF pulse sequence. The spectrum in Fig. 6b was acquired with the STEAM-SLR RF pulse sequence. The contamination of the lipids from the skull marrow was greatly reduced in the SLR sequence compared with that in the sinc sequence. The same effect was observed in the other volunteers. In the case of spectroscopy of tumors located close to the skull marrow, water-suppressed ^{1}H MR spectroscopy using sinc RF pulses will result in more severe overlap of lipids with lactate versus a sequence using SLR RF pulses.

CONCLUSIONS

The new set of RF pulses numerically optimized using the Shinnar–Le Roux algorithm exhibits voxel profiles that are closer to ideal than those of the standard Hamming-filtered sinc RF pulses. With these new pulses, the PRESS voxel profile is now greatly improved such that STEAM and PRESS now excite a voxel of nearly the same shape and size—the PRESS sequence no longer excites a much smaller volume with inferior voxel profile as compared with STEAM.

The STEAM-SLR sequence is shown to be less sensitive to flip angle errors than the PRESS-SLR sequence. With STEAM, $\theta < 90°$ simply results in a theoretically expected decrease in signal, with a constant decrease in signal across the voxel. For $\theta > 90°$, nonlinearities in the voxel profile result with the total signal still scaling as predicted theoretically. With PRESS-SLR, nonlinearities in the voxel profile result for $\theta \neq 90°$ with the total signal not following theoretical predictions of scaling with flip angle (maximum total signal occurs for $\theta = 75°$). For PRESS-SLR, the 90° flip angle must not be set by maximizing the spectroscopic signal from the voxel. Setting the proper flip angle by simply observing the spectrum is not recommended. Compared to the simple flip angle dependences with hard-pulse STEAM and PRESS sequences, our results showed a complex relationship between the integrated signal and flip angle with the SLR RF pulses.

In vivo results from healthy volunteers demonstrate re-

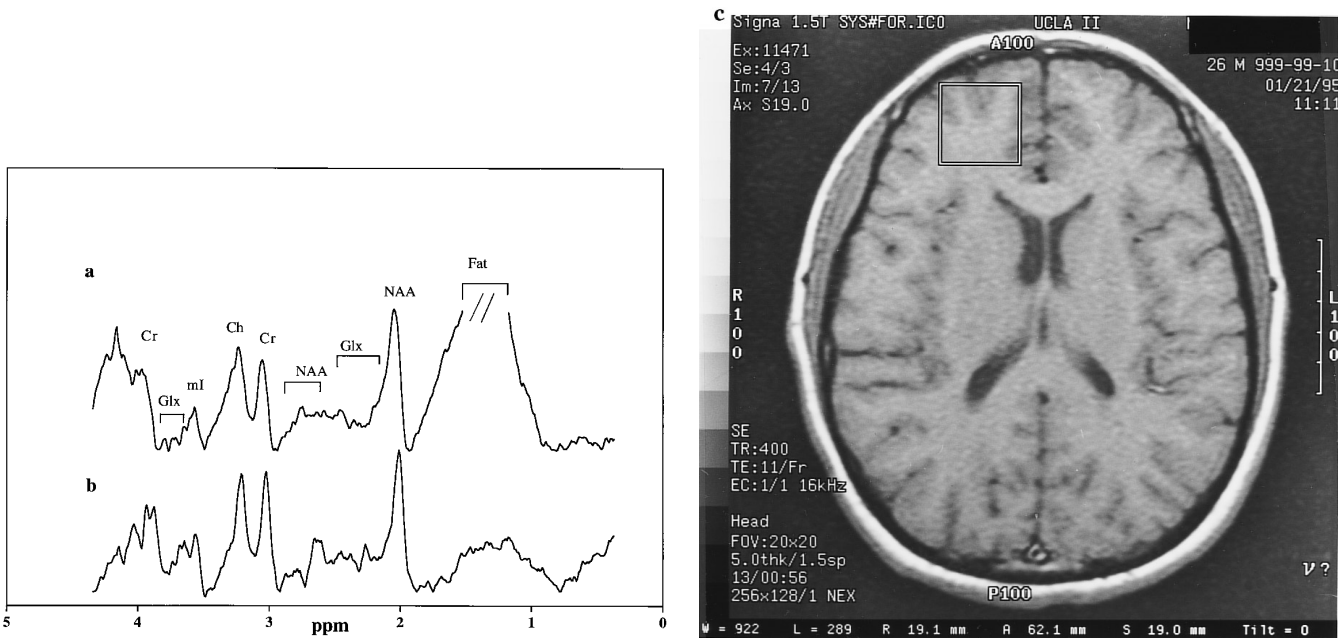

FIG. 6. Water-suppressed ^{1}H MR spectra from identical locations in the frontal lobe of a healthy volunteer: (a) STEAM-sinc and (b) STEAM-SLR. An 18-ml voxel was localized in the frontal white/gray matter. TR = 1500 ms, TE = 20 ms. Number of excitations = 128. (c) MR axial image of a healthy volunteer showing the voxel location for MRS.

duced lipid contamination in voxels selected close to the skull when using the optimized SLR RF pulses versus the standard sinc RF pulses.

ACKNOWLEDGMENTS

This work was supported by a grant from the Whitaker Foundation. The authors acknowledge the generous support and encouragement of Professor J. A. Sorenson of the Department of Medical Physics and Radiology, University of Wisconsin, Madison, and Dr. Richard Steckel of the Department of Radiological Sciences, University of California, Los Angeles. The authors also thank Dr. Patrick Turski of the University of Wisconsin, Madison, for his support.

REFERENCES

1. M. S. Silver, R. I. Joseph, and D. I. Hoult, Highly selective 90° and 180° pulse generation, *J. Magn. Reson.* **59,** 347–351 (1984).
2. D. J. Lurie, A systematic design procedure for selective pulses in NMR imaging, *Magn. Reson. Imaging* **3,** 235–243 (1985).
3. V. M. Runge, M. L. Wood, D. M. Kaufman, and M. S. Silver, MR imaging section profile optimization: Improved contrast and detection of lesions, *Radiology* **167,** 831–834 (1988).
4. J. W. Carlson, Exact solutions for selective-excitation pulses, *J. Magn. Reson.* **94,** 376–386 (1991).
5. M. Garwood, T. Schleich, and M. R. Bendall, Simulation of selective pulse techniques for localized NMR Spectroscopy, *J. Magn. Reson.* **73,** 192–212 (1987).
6. J. Mao, T. H. Mareci, and E. R. Andrew, Experimental study of optimal selective 180° radiofrequency pulses, *J. Magn. Reson.* **79,** 1–10 (1988).
7. S. Conolly, D. Nishimura, and A. Macovski, Optimal control solutions to the magnetic resonance selective excitation problem, *IEEE Trans. Med. Imaging* **5,** 106–115 (1986).
8. J. M. Pauly, P. Le Roux, D. Nishimura, and A. Macovski, Parameter relations for the Shinnar–Le Roux selective excitation pulse design algorithm, *IEEE Trans. Med. Imaging* **10**(1), 53–65 (1991).
9. P. Xu, X. L. Wu, and R. Freeman, User-friendly selective pulses, *J. Magn. Reson.* **99,** 308–322 (1992).
10. P. R. Luyten, A. J. H. Marien, and J. A. Den Hollander, Acquisition and quantitation in proton spectroscopy, *NMR Biomed.* **4,** 64–69 (1991).
11. J. Frahm, K. D. Merboldt, and W. Hanicke, Localized proton spectroscopy using stimulated echoes, *J. Magn. Reson.* **72,** 502–508 (1987).
12. P. Bottomley, U.S. Patent 4 480 228 (1984).
13. P. C. M. van Zijl, C. T. W. Moonen, J. R. Alger, J. S. Cohen, and S. A. Chesnick, High-field localized proton spectroscopy in small volumes: Greatly improved localization and shimming using shielded strong gradients, *Magn. Reson. Med.* **10,** 256–265 (1989).
14. C. T. W. Moonen, M. von Kienlin, P. C. M. van Zijl, J. Cohen, J. Gillen, P. Daly, and G. Wolf, Comparison of single-shot localization methods (STEAM and PRESS) for in vivo proton NMR spectroscopy, *NMR Biomed.* **2,** 201–208 (1989).
15. C. T. W. Moonen and P. C. M. Van Zijl, Highly effective water suppression for *in vivo* proton NMR spectroscopy (DRYSTEAM), *J. Magn. Reson.* **88,** 28–41 (1990).
16. J. Frahm, H. Bruhn, M. L. Gyngell, K. D. Merboldt, W. Hanicke, and R. Sauter, Localized high-resolution proton NMR spectroscopy using stimulated echoes: Initial applications to human brain in vivo. *Magn. Reson. Med.* **9,** 79–93 (1989).
17. P. Webb, Application of crafted pulses to *in vivo* spectroscopy, *in*

Abstracts of the Society of Magnetic Resonance in Medicine, 11th Annual Meeting, p. 2131 (1992).

18. Y. Ke, L. N. Ryner, and M. A. Thomas, Flip angle effects in STEAM and PRESS: SLR vs sinc rf pulses, *in* Abstracts of the Society of Magnetic Resonance, 3rd Annual Meeting, p. 1019 (1995).

19. R. E. Hurd and N. Sailasuta, Elimination of artifacts in short echo proton spectroscopy, *in* Abstracts of the Society of Magnetic Resonance in Medicine, 5th Annual Meeting, p. 1453 (1997).

20. I. R. Young, G. M. Bydder, and J. A. Payne, Variations in slice shape and absorption as artifacts in the determination of tissue parameters in NMR imaging, *Magn. Reson. Med.* **2,** 355–389 (1985).

21. M. R. Bendall and D. T. Pegg, Uniform sample excitation with surface coils for *in vivo* spectroscopy by adiabatic rapid half passage, *J. Magn. Reson.* **67,** 376–381 (1986).

22. K. Ugurbil, M. Garwood, and M. R. Bendall, Amplitude- and frequency-modulated pulses to achieve 90° plane rotations with inhomogeneous B_1 fields, *J. Magn. Reson.* **72,** 177–185 (1987).

23. A. J. Johnson, M. Garwood, and K. Ugurbil, Slice selection with gradient-modulated adiabatic excitation despite the presence of large B_1 inhomogeneities, *J. Magn. Reson.* **81,** 653–660 (1989).

24. M. Garwood and Y. Ke, Symmetric pulses to induce arbitrary flip angles with compensation for RF homogeneity and resonance offsets, *J. Magn. Reson.* **94,** 511–525 (1991).

25. G. K. Radda, The use of NMR spectroscopy for the understanding of disease, *Science* **233,** 640–654 (1986).

26. P. Blondet, M. Decorps, S. Confort, and J. P. Albrand, ^{1}H *in vivo* NMR spectroscopy with surface coils. Hard-pulse water suppression sequences and spatial localization, *J. Magn. Reson.* **75,** 434–451 (1987).